IEEE Access
Multidisciplinary | Rapid Review | Open Access Journal

Received 5 August 2023, accepted 1 September 2023, date of publication 8 September 2023, date of current version 18 September 2023.

Digital Object Identifier 10.1109/ACCESS.2023.3313553

RESEARCH ARTICLE

An Adaptive Regenerative Braking Strategy Design Based on Naturalistic Regeneration Performance for Intelligent Vehicles

MARWA ZIADIA[1], SOUSSO KELOUWANI[2], (Senior Member, IEEE), ALI AMAMOU[2], (Member, IEEE), AND KODJO AGBOSSOU[2], (Senior Member, IEEE)

[1]Department of Mechanical Engineering, Hydrogen Research Institute, Université du Québec à Trois-Rivières, Trois-Rivières, QC G8Z 4M3, Canada
[2]Department of Electrical and Computer Engineering, Hydrogen Research Institute, Université du Québec à Trois-Rivières, Trois-Rivières, QC G8Z 4M3, Canada

Corresponding author: Marwa Ziadia (marwa.ziadia@uqtr.ca)

This work was supported in part by the Foundation of Université du Québec à Trois-Rivières, Canada Research Chair Program; and in part by the Natural Sciences and Engineering Research Council of Canada.

ABSTRACT The effectiveness of regenerative braking strategies plays an important role in extending the driving range of electric vehicles. Since the driver is still an essential factor in levels 3 and 4 of intelligent electric vehicles, improving user acceptance and adoption of the braking control strategy is crucial. This paper puts forward a new regenerative braking strategy to find a compromise between optimal braking control performance and naturalistic regeneration performance while satisfying the maximum speed preference when driving between two-stop events. Unlike other similar works that only maximize regenerative braking energy while satisfying the physical limits of an electrified powertrain, this paper considers naturalistic regeneration performance. To achieve this, firstly, the power regenerated by three drivers is predicted with a long-horizon (30 seconds), using long-short-term memory networks (LSTM) and non-linear autoregressive exogenous model (NARX). Subsequently, an estimation of the energy recovery maximization rate is performed to give a perception of the naturalistic regeneration performance. As this performance varies, the deceleration planning employs three horizon scales of long, medium, and short, determined by the energy recovery maximization rate. Finally, dynamic programming (DP) is utilized to optimize a deceleration profile. The study utilizes real data of inverter efficiency, transmission efficiency, and motor-to-battery efficiency map. The outcome of this study shows that the proposed regeneration braking strategy is adaptive, improving regeneration efficiency by 39,6% for driver 1, 16% for driver 2, and 26% for driver 3, and forecasting the optimality of some deceleration behaviors.

INDEX TERMS Eco-driving, acceptance, driving behaviors, regenerative braking, intelligent vehicles, machine learning, optimal control.

I. INTRODUCTION

Transport is the second greatest energy user and emitter of carbon dioxide. Pure electric vehicles provide a solution to this environmental challenge, despite their limited driving range and long recharging time [1], [2]. As city populations and densities rise, traffic congestion, and the risk of accidents increase as well. In response to these challenges, academia and businesses have redoubled their efforts to develop and perfect autonomous electric vehicles (AEVs) [3], [4]. AEVs are considered a crucial requirement for greener, safer, and more efficient urban transportation [5]. Smart decision-making in AEVs allows them to maximize profits and minimize energy consumption by wisely managing and trading among available energy sources [6].

The eco-driving system includes diverse strategies that optimize the driving velocity profile to significantly reduce energy consumption [7]. Studies examining navigational data, high-precision map data, and energy consumption data have shown that combining eco-driving technology with

The associate editor coordinating the review of this manuscript and approving it for publication was Jie Gao.

connected and automated vehicles (CAVs) can have a significant impact on energy consumption. Adequate speed controls can be achieved by utilizing background information such as speed limits, safe speeds for curved roads, and an estimate of the average traffic speed. The speed planning problem can be formulated as an optimal control problem with the objective of reducing energy consumption while considering the constraints imposed by the mapping information [8]. However, real-time deployment of such systems is inhibited by algorithmic limitations resulting from factors like unexpected nearby car maneuvers, inevitable traffic congestion, intermittent data connectivity, and so forth. Moreover, global optimization search algorithms, including model dynamic programming (DP) and Pontryagin's minimum principle (PMP), require high computational costs that are not currently provided by existing vehicle computing units [7], [9], [10], [11]. Due to unforeseen circumstances, optimal solutions calculated over the whole path may be invalid or reduce the real-time powertrain's energy efficiency [12]. Even though the G7 nations have decided to eliminate the legal barriers impeding the development of autonomous cars, these vehicles are still far from being widely accepted in society. Golbabaei et al. [13] have demonstrated significant differences in public perceptions and adoption intentions among various sociodemographic subgroups. Researchers have also shown that travelers are more likely to ride entirely in autonomous vehicles (AVs) under monotonous driving conditions, such as highways, than in urban conditions. In contrast, most consumers are willing to acquire AEVs equipped with a level 2 or 3 advanced driver-assistance system (ADAS), despite the fact that such vehicles are not fully autonomous and charging facilities are insufficient, particularly at the end of 2022 with the inflation of fuel costs [10], [11]. These levels of automation have the same potential for improving energy efficiency as level 5 ADAS due to the same perception sensors.

Given the aforementioned considerations, improving the performance of level 2 or level 3 autonomous driving systems in real-time operation is crucial, as this can help extend the autonomy of electric vehicles. Researchers have developed various eco-driving strategies that can be categorized in terms of their application to specific environments, such as eco-cruising on highways and eco-approach at signalized intersections [14], [15]. Through the analysis of the junction's signal phase and timing (SPaT), the vehicle's data, and the traffic flow, the eco-Approach and Departure (EAD) program determines the most energy saving way to pass through the intersection [16]. Furthermore, researchers have mostly focused on improving eco-driving performance in real-time by concentrating on more restricted driving scenarios, such as regenerative brake control, acceleration and deceleration (vehicle tracking), and speed restriction based on traffic signs. Han et al. [17] have developed an optimal control problem for acceleration or deceleration while satisfying safety constraints, minimum inter-vehicle distance, and maximum speed limit, considering the presence of vehicles in front. Yang et al. [18] have specifically developed a vehicle queuing process at signaled intersections using the shock wave profile model to create a green window for planning eco-course vehicles in a congested environment. Zhao et al. [19] have presented a predictive model using the receding horizon to reduce platoon fuel consumption and pass the junction on a green phase. The authors claim that the proposed model achieves eco-driving without considering the optimal regeneration performance. Energy recovery using power from regenerative braking is one of the most common strategies to improve fuel economy for electric vehicles (EVs) [20], [21]. This energy recovery process involves converting the kinetic and potential energies to electric power using the traction motor as a generator [22], [23]. Apart from the importance of considering the optimal speed profile to minimize energy consumption, it is also essential to improve energy recovery performance [24]. Extensive studies have focused on the regenerative torque distribution (RTD) strategy to maximize the braking energy recovery without compromising braking performance, safety, and driveability [20], [25], [26]. Owing to the energy efficiency-centric design of HEVs and EVs, comfort is among the most important criteria. However, powertrain, drivetrain, and comfort optimization are mostly related to the vehicle manufacturer's design, with little control given to the driver when considering the comfort settings. The vehicle motion profile is one factor that affects comfort (i.e., acceleration, deceleration) [27]. Therefore, acceleration and braking actions need to be constrained to provide a comfortable driving experience.

In light of recent studies, the performance of a regenerative system, acceleration, and deceleration is impacted by several factors, such as the variation of operation conditions, road topology, traffic volume, weather conditions, and driving behaviors. In such circumstances, many researchers have focused on anticipating future events to minimize irreversible driving errors under varying road conditions [28], [29]. In [30], a model predictive control (MPC) is designed using the acceleration prediction of the car in front by NARX model. Given this information, the MPC optimizes both speed tracking and energy recovery rate for the new method of adaptive cruise control. In [31], an MPC- based tire dynamics and vehicle load control method is proposed to increase the regeneration efficiency of electric machines and reduce tire slip loss. In [32], Q-learning algorithms create optimal speed profiles while stopped at red lights by considering all relevant real-time parameters via vehicle-to-infrastructure (V2I) communication. Better results are achieved by experimental verification of the predicted speed profiles that determine the braking actions of vehicles in response to varying road conditions. In [33], a hybrid method termed as Layer Hidden Markov Model-Dynamic Compensatory Fuzzy Neural Network is used to recognize the driver's braking intention with the goal of improving braking sense and increasing the amount of energy that can be recovered. In [34], personalized

and green adaptive cruise control for intelligent electric vehicles is presented to improve regenerative braking and ADAS comfort. It is optimized via nonlinear MPC theory and uses the Hammerstein model with key parameters that vary according to driving style. Therefore, several improvements in regeneration systems have been proven in the literature by anticipation of future events and driving styles, but the relation of driving style, regeneration performance, and acceptability of ADAS has not been explored sufficiently [35]. From a technical perspective, efficient driving with EVs mainly depends on anticipatory braking conditions, and the EVs engine operates optimally at a higher speed. Therefore, coasting as much as possible is relevant to optimize energy recovery. Also, the anticipation of the braking phase during the vehicle movement has several benefits as the vehicle moves. It makes it possible to prepare the recovery mechanism to recover the maximum kinetic energy.

Since regenerative braking only works with technically limited efficiency, the amount of kinetic energy that will be converted back to electricity and stored in the battery is mainly dependent on the driving style [36], [37], [38], the physical limitations of motor generation, and the deceleration limitations of regenerative braking. Some works in the literature regarding the maximization of regeneration respect the motor's physical limit [39]. In [40], real driving test data characterizing the physical limits of regenerative braking are used to propose an energy-optimal deceleration planning system and improve energy-recuperation efficiency gains. Such strategies are employed in formulating ADAS, mainly used by autonomous vehicles of level 5. However, they cannot be very effective when integrated into autonomous vehicle level 3 or 4, where the driver is an essential factor, and driver acceptance of braking control strategies presents a challenge in the literature [41]. In reality, when approaches do not consider individual naturalistic regeneration performance in the brake control optimization model, it can sometimes lead to painful and circumvent excessive and bothersome alerts, which often lead drivers to disengage the system, thereby directly impacting its efficiency [42]. This performance is evaluated by the capability to energy regenerate up to the engine's regeneration limit while respecting maximum speed preferences [43]. To manage standard control strategies, an adaptive method will be extremely important [44], [45]. Thus, this paper has two major contributions: (i) This research predicts the power regenerated by drivers over a long horizon (30 seconds), utilizing LSTM and NARX models. These models effectively predict the performance of naturalistic regeneration and estimate whether the deceleration behavior within this context is optimal or requires assistance. (ii) Adding the forecasting of driver naturalistic regeneration performance to regenerative braking strategy design is the main contribution of this work. Recognizing the variable nature of this performance, our proposed braking strategy maximizes regenerative energy to the physical limits of an electrified powertrain by adapting the deceleration planning horizon to the driver's naturalistic regenerative performance. This adaptive regenerative braking strategy is very useful within the context of eco-friendly braking assistance. Contrary to most of the existing papers in the literature, which are based on simulation, the results obtained of this work have been validated with real data of inverter efficiency, transmission efficiency, and motor-to-battery efficiency map of Kia Soul 2017.

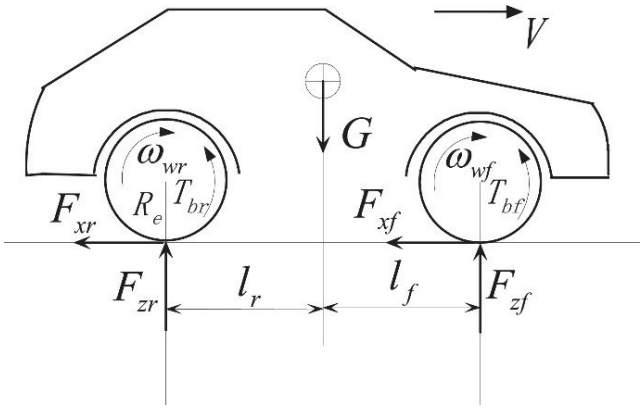

FIGURE 1. The vehicle braking model [46].

The rest of this article is organized as follows. Section II describes the electric vehicle model that was used to compute deceleration distance and power regeneration. Section III explains the proposed braking control strategy adaptation algorithm. The experimental results are reported and discussed in section IV. Finally, the conclusion is given in section V.

II. ELECTRIC VEHICLE MODEL TO CALCULATE DECELERATION DURATION AND POWER REGENERATION

A. VEHICLE DYNAMICS MODEL

Regenerative braking controllers require a vehicle dynamics model. Since the electric vehicle's braking performance is the focus of this paper's attention, the vehicle dynamics model is simplified to longitudinal motion, assuming straight braking and no steering effect. The vehicle dynamics model, including longitudinal and rotational wheel movement illustrated in Fig. 1, can be described as follows:

$$\begin{aligned} M\dot{v}(t) &= F_{xf}(t) + F_{xr}(t) + F_{\text{Load}}(t) \\ F_{\text{Load}}(t) &= F_{\text{Load},\alpha}(t) + F_{\text{Load},\beta}(t) \\ F_{Brk}(t) &= -F_{xf}(t) - F_{xr}(t) \end{aligned} \tag{1}$$

where $F_{\text{Load},\alpha}$ and $F_{\text{Load},\beta}$ are defined as:

$$\begin{cases} F_{\text{Load},\alpha}(v,\theta) = C_0\cos(\theta(X(t))) + C_1 v(t) + C_2 v^2(t) \\ F_{\text{Load},\beta}(\theta) = Mg\sin(\theta(X(t))) \end{cases} \tag{2}$$

M is the total mass of the vehicle, v is the longitudinal vehicle velocity, θ is the road slope, F_{xf} and F_{xr} are respectively the longitudinal tire-road friction forces at the front and rear tires. C_0 and C_1 are rolling resistance coefficients, C_2 is

an aerodynamic coefficient, and $X(t)$ represents the location in the time domain. Numerical values of these coefficients are obtained from real driving tests on normal road surface conditions.

The tire-road friction force is calculated as follows:

$$F_{xj}(t) = \mu_j(\kappa) F_{zj}(t) \tag{3}$$

where F_{zj} represents the normal load on tires, and μ_j is the tire-road friction coefficient as a function of the slip ratio. Pacejka [47] developed a model to express the tire-road friction coefficient as a non-linear function of the slip ratio, as follows:

$$\mu_j(\kappa) = D_x \sin\left\{C_x \arctan\left[B_x\kappa_j - E_x\left(B_x\kappa_j - \arctan\left(B_x\kappa_j\right)\right)\right]\right\} \tag{4}$$

where B_x, C_x, D_x, E_x are the stiffness, shape, peak, and curvature factor, respectively. The longitudinal slip ratio κ_j, which defines the difference in longitudinal velocity between the wheel axle and tires rotational velocity, is derived as follows:

$$\kappa_j = \frac{\omega_{wj} R_e - v(t)}{v(t)} \tag{5}$$

where R_e is the effective rolling radius of the tires, and ω_{wj} is the rotary velocity of front and rear wheels. According to this, the normal load on front and rear tires is dependent on the longitudinal deceleration (a_x).

$$\begin{aligned} F_{zf} &= \frac{M\left(l_r g - h a_x(t)\right)}{l_f + l_r} \\ F_{zr} &= \frac{M\left(l_f g + h a_x(t)\right)}{l_f + l_r} \end{aligned} \tag{6}$$

where l_f and l_r are the longitudinal distances from the center of gravity to the front and rear tires, g is the acceleration due to gravity, and h is the distance from the center of gravity to the vehicle's ground.

B. VEHICLE DECELERATION DURATION

The speed profile is a temporal and spatial process, which makes $v(X(t))$ represent the speed profile at a specific observation station (i,e, location) at time t. Given a sequence of speeds at $X_i(t)$ values, the speed profile to arrive at $X_i(t + \Delta(t))$ can be accurately estimated after a time interval $\Delta(t)$. Furthermore, the speed profile and deceleration duration can be described as follows:

$$v_{i+1}(t) = v_i(t) + \frac{F_{xf}(\mathrm{t}) + F_{xr}(\mathrm{t}) + F_{L_{\mathrm{Load}}}(t)}{m}\Delta t_i \tag{7}$$

$$v_{i+1}^2 = v_i^2 + \frac{2\Delta X_i}{m}\left(F_{xf} + F_{xr} + F_{\mathrm{Load}}\left(v_i^2, \theta_i\right)\right) \tag{8}$$

$$v_{i+1} = \sqrt{\frac{2\Delta X_i}{m}\left(F_{xf} + F_{xr} + F_{\mathrm{Load}}\right) + v_i^2} \tag{9}$$

$$t_{i+1} = t_i + \frac{\Delta X_i}{v_i} \tag{10}$$

$$t_N = \sum_{i=0}^{N-1} \frac{\Delta X_i}{v_i} \tag{11}$$

where $F_{\mathrm{Load}}\left(v_i^2, \theta_i\right)$ is affine in v_i^2, and t_N is the duration decelaration. In this case, we use the formula $v_i = v(t_i) = v(X(t_i)) = v(X_i)$, which is also used for other dependent variables.

C. MOTOR AND BATTERY MODELS

According to Xu et al. [46], the output torque of electric motors is amplified and exerted on the wheels through the reduction gear. Therefore, the rotational velocity of four small high-power in-wheel motors is decreased. The governing equations can be expressed as:

$$\begin{aligned} T_w &= g_0 T_m \\ \omega_w &= \frac{1}{g_0} \cdot \omega_m \end{aligned} \tag{12}$$

where T_w is the braking torque on the wheels, T_m is the actual motor torque, ω_w is the rotational velocity of the wheels, ω_m is the rotational velocity of the motors, and g_0 is the transmission ratio of the reduction gear.

The simplification of the braking torque on the wheels (T_w) can be expressed as a first-order reaction model with a small-time constant τ:

$$T_w = g_0 \cdot \frac{1}{\tau s + 1} \cdot T_{m,\,\mathrm{ref}} \tag{13}$$

where $T_{m,\,\mathrm{ref}}$ is the reference motor torque. The motor-to-battery regenerative braking efficiency η depends on the braking torque and rotational velocity of the in-wheel motors:

$$\eta = \eta\left(T_m, \omega_m\right) = \frac{U_c I_C}{T_m \omega_m} \tag{14}$$

where U_c and I_c are respectively the battery charging voltage and current of one in-wheel motor.

The battery provides the requested power for the in-wheel motors. The average battery model consists of an open-circuit voltage and an internal resistance, which are a function of the state of charge (SOC) and the temperature. The battery regenerative power P_r is given by:

$$\begin{aligned} P_r &= U_b I_b \\ P_r &= T_b \omega_b \end{aligned} \tag{15}$$

where U_b is the terminal voltage and I_b is the current of the battery. Battery SOC measures the effective discharge rate, which is estimated by the coulomb counting:

$$SOC^t = SOC^0 - \frac{100}{C_n} \times \int_0^t I\left(\frac{I}{I_n}\right)^{pc-1} dt \tag{16}$$

where C_n is the nominal capacity measured at nominal current (I_n) predefined by the manufacturer. SOC^t represents the SoC value at time t. and pc is Peukert's constant typically measured empirically for the type of lithium-ion battery cell.

D. GENERALIZED ENERGY RECUPERATION MODEL

The regenerative deceleration force of an electric vehicle is limited by the electric motor's regenerating capacity. Additionally, the regenerative braking force depends on the electric vehicle's motor configuration. The regenerative-braking force can be limited as follows:

$$F_{RQn} = \max\left(F_{Brk}, F_{Lmt}\right) \tag{17}$$

where the limit of powertrain's regeneration force (including the traction motor and gearbox) is given by:

$$F_{Lmt}(v) = \frac{1}{r_w} T_{Lmt}(v) g_i(v) g_f \tag{18}$$

where T_{Lmt} is the torque limits of the electric motor in regenerator-mode, r_w is the dynamic wheel radius, $g_i(v)$ is the gearbox ratio determined by the gear-shift controller based on the current longitudinal vehicle speed v. T_{Lmt} can be obtained by performing a quasi-steady-state, equivalent to the following mathematical expression:

$$T_{Lmt}(v) = f\left(\omega_{Mot}(v)\right) \tag{19}$$

where T_{Lmt} is the motor rotation speed in RPM.

III. ADAPTIVE ENERGY DECELERATION PLANNING SYSTEM DESIGN

The proposed strategy in this paper is called Adaptive Energy Deceleration Planning System (AEDPS). AEDPS aims to optimize and adapt deceleration planning by considering two crucial factors: the individual's naturalistic regeneration performance and the driver's maximum speed preferences. Fig. 2 illustrates the general structure of AEDPS, which comprises three essential components: long-horizon forecasting of power specific to each driving behavior, determination of the energy recovery maximization rate, and adaptive optimal deceleration planning. AEDPS requires power forecasts for a relatively long horizon of 30 seconds since determining the high energy recovery maximization rate in advance is necessary for deceleration planning with a long horizon. To account for the two effects mentioned above, the strategy estimates the amount of energy that can be maximized and determines the most appropriate deceleration planning horizon during the optimization phase of the deceleration profile. It utilizes three horizon scales: long, medium, and short. The long horizon is used to develop long-term deceleration profiles and improves regeneration for a high energy recovery maximization rate. Medium and short horizons are utilized for moderate and minimal energy recovery maximization rates, respectively. In the case of optimal naturalistic deceleration behaviors, the strategy disables the control warning from ADAS to the drivers The development of each component is described in detail below.

A. ANALYSIS AND PREDICTION OF POWER

In this section, the experimental setup, fixed-route driving for data collection, and data preprocessing are explained. The last subsection introduces the two-time series prediction models used in this strategy and the correlation analysis between power consumption and driving behaviors.

TABLE 1. Key parameters of the electric vehicle.

Parameter Name	Symbol	Value
Vehicle mass	M	1490 kg
Height of vehicle c.g.	h	0.25 m
Distance from c.g. to front axle	l_f	1.2 m
Distance from c.g. to rear axle	l_r	1.4 m
Effective radius of the tire	R_e	0.31 m
Reducer ratio	g_0	8.2
Battery voltage	V_{bat}	360 V
Battery capacity	Bat_{cap}	75 Ah
Max. speed	V_{MA}	145 km/h
Drag coefficient	C_d	0.35
Rolling resistance of dry road	μ	0.012
Air Density	ρ	0.80795 kg/m3
Gravitational acceleration	g	9.8 m/s2
Vehicle deceleration rate	a_x	0.3 m/s2

1) EXPERIMENTAL SETUP FOR DATA COLLECTION

An instrumented 2017 Kia Soul intelligent electric vehicle (EV) was utilized for the collection of naturalistic driving data, in-vehicle information, and environmental factors. The vehicle's parameters are summarized in Table1. As depicted in Fig. 3, the onboard measurement system comprises the global positioning system (GPS), the onboard diagnostic system (OBD), and the ADAS system installed in the experimental vehicle. The GPS system, Septentrio (AsteRx-i3 D Pro+), mounted in the vehicle's trunk, was chosen for its good real-time accuracy, which is ideal for calculating vehicle position and road parameters. This high level of accuracy is achieved using the Real-time Kinematic (RTK) approach, which enhances the Global Navigation Satellite System (GNSS) accuracy and utilizes an RTCM correction stream. Furthermore, AsteRx-i3 D Pro+ integrated GNSS-IMU system with a dual antenna, multi-frequency GNSS receiver, and a Vectornav VN-100 micro-electromechanical system (MEMS) IMU was used to get the ground truth [48]. Specifically, the GNSS receiver uses a Kalman filter algorithm to merge IMU and GNSS data for precise location and reliable GNSS/INS positioning and 3D orientation. Fig. 3 shows the OBDlinkMx and Mobileye systems connected to the OBD2 ports for CAN-Bus communication. The OBDlinkMx operates via Bluetooth on PCs and is responsible for collecting vehicle parameters such as brake and acceleration pedal states, motor torque, etc. The Mobileye system, securely mounted and calibrated at the center of the windshield, operates using an intelligent digital camera powered by the EyeQ chip. This advanced system provides high-performance, real-time image processing capabilities, enabling the detection of vehicles, lanes, pedestrians, and traffic signs, including stop signs. It also efficiently calculates the dynamic distance between the vehicle and other road objects. Furthermore, Mobileye can recognize obstacles at a longitudinal distance of up to 250 m from the reference point.

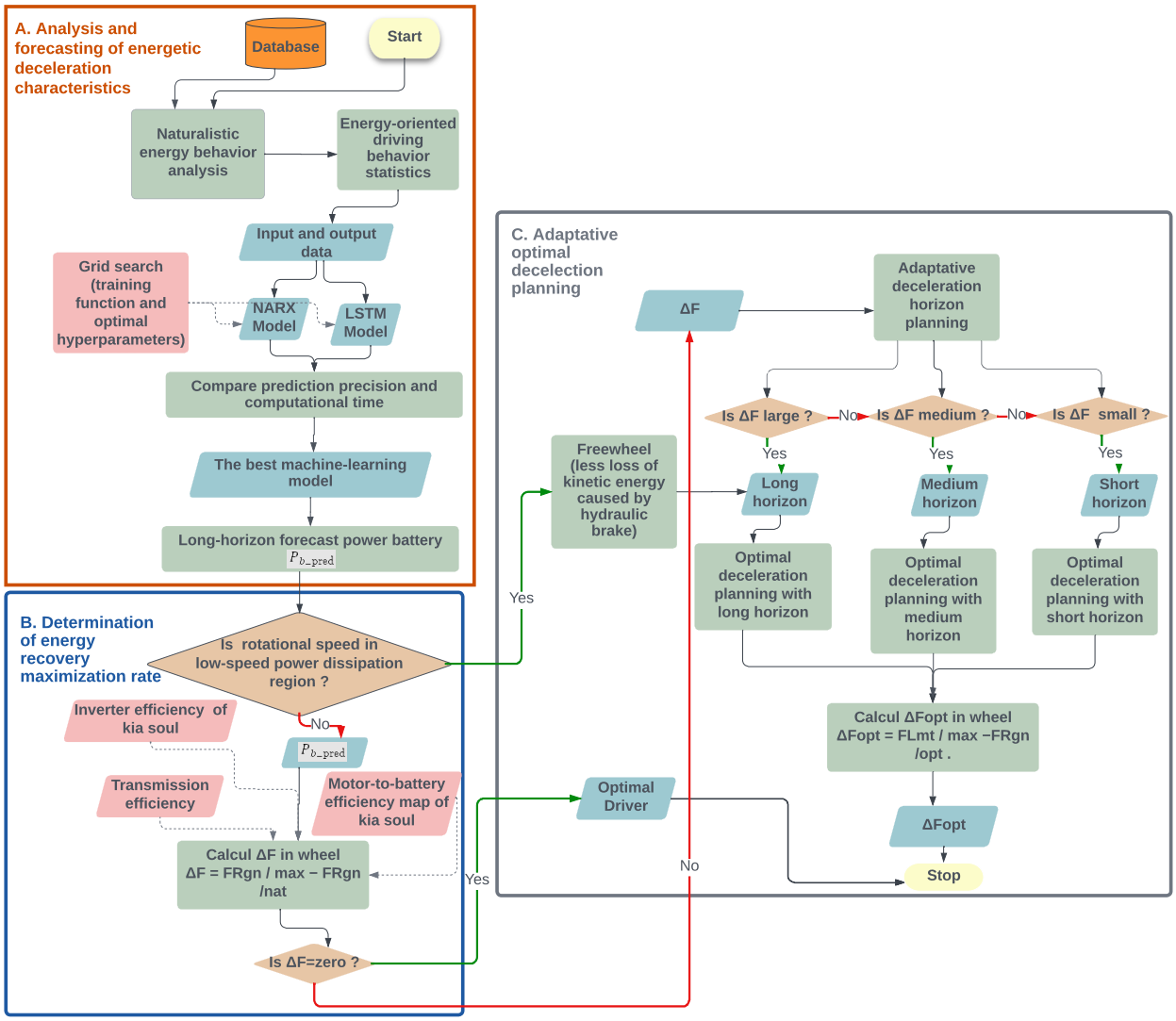

FIGURE 2. AEDPS Design.

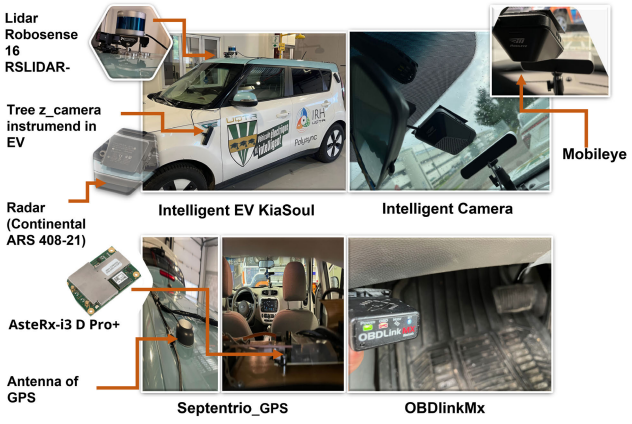

FIGURE 3. Instrumented intelligent electric vehicle (Kia Soul 2017).

2) FIXED-ROUTE NATURALISTIC DRIVING DATA COLLECTION

This study employs the fixed route that is applicable to vehicles in which the driver takes the same route to work or commercial vehicles, such as city buses and garbage trucks, that mostly commute on the same routes at the same time. The selection of fixed routes in this study is used to improve the forecasting of variation in driving behaviors on-road characteristics. Naturalistic driving data are collected on the same route (Trois-Rivières, Quebec) to study the deceleration and braking patterns in a real traffic environment. The database has been checked under the following conditions:

- There were no surrounding vehicles, traffic lights, and dynamic obstacles.
- The braking events are initiated by static obstacles, such as stop signs and static objects detected by Mobileye.
- The route has covered a total distance of 4 km.
- The selection of the road has been made mainly because of the substantial amount of stop panels (12 stop signs).

The experiment session began once a participant was confident about driving the test vehicle safely. Multiple drivers performed the experiments, and an assistant in the vehicle gave the participants route guidance instructions

to synchronize the start of data collection from all the instruments.

3) JOINT FEATURE LEARNING AND TIME SERIES MODELING

Using the developed EVs dynamic model, a dataset with known inputs and outputs can be obtained which opens up an opportunity for using supervised machine learning to develop an inferred function. In this regard, two recurrent neural networks (RNN)-based methods, namely LSTM and NARX, are used herein to long-horizon forecast the power of the EVs under study. The recurrent structure of the mentioned methods allows them to exhibit the temporal dynamic behavior caused by the driving conditions of the EVs. NARX has already been used successfully to predict time series in different applications [49]. It can forecast a time series future value based on its current and past values as well as another time series' past and current values, known as an external or exogenous time series. NARX can model and rapidly converge to time-sequential vehicle states. However, it suffers from long-term dependence and does not detect information in sequential data. This limitation is due to its vulnerability to the vanishing gradient problem. Hochreiter and Schmidhuber developed the LSTM to address the mentioned shortcomings. LSTM has three gates, an input gate, an output gate, and a forget gate, which can improve its performance in long-term learning tasks [38], [50], [51]. This option is considered critical because this network is prone to overfitting. The vulnerability of LSTM is the need for significant memory. Another drawback is that it necessitates more computing power than the NARX network. A comparison of the two methods will be presented in this study to identify the best neural network for predicting braking power.

Datasets with a high number of variables are frequently challenging to summarize or analyze. To address this, Principal Component Analysis (PCA) was performed to reduce the dimensionality of the dataset used in the forecasting model. The correlations between the principal components and the original variables are presented in Table 2. It can be seen that there is no correlation between the principal components themselves. The first principal component is highly correlated with six variables of the original ones. The first principal component increases with increasing Battery Current, Battery Voltage, Battery Power, Motor Torque, and lightly with distance to stop and Speed scores, suggesting that these six criteria vary together. If one increases, then the remaining ones tend to increase as well. Furthermore, the first principal component correlates strongly with the battery variables. The second principal component increases with the rotational speed and its equivalent speed. However, the second main component correlates strongly with the road characteristics provided by the GPS. The outcome of this process indicates that the followings features are discriminative: the speed χ_1, the distance to the next stop panel χ_2, the Motor Torque χ_4, the Latitude χ_5, the Altitude χ_6 and the Rotational Speed χ_7. The Battery Power signal is used as the output ($y(1)$).

TABLE 2. Extracted vectors.

Data	Coefficients of PC1	Coefficients of PC2
Speed	**0,23125**	**0,32684**
Distance to Stop	**0,32548**	,19156
Longitude	0,07202	**-0,56701**
Latitude	0,06528	**0,29689**
Altitude	-0,09792	**0,54841**
Battery Current	**0,45743**	0,01558
Battery Voltage	**-0,4649**	-0,02672
Battery Power	**0,45818**	0,01615
Rotational Speed	0,17716	**0,33945**
Motor Torque	**0,39247**	-0,07497
Acceleration	-0,02749	-0,15498

The prediction results are evaluated using two different accuracy measures: the root-mean-square-error (RMSE) and the computational time. RMSE is a regularly used index to quantify model regression performance, with scale-dependent measurement and evaluation for sequence prediction. Additionally, the model should not produce computationally expensive results. This is why it is equally critical to assess training time. The root mean squared error RMSE is defined as:

$$\mathrm{RMSE} = \left\{ \frac{1}{N} \sum_{t=1}^{N} \left(\hat{y}_t - y_t \right)^2 \right\}^{1/2} \tag{20}$$

where $\hat{y}_t$ and y_t present predicted and actual battery power of vehicles usages for N discrete time samples. A comparison of the prediction performances of LSTM and NARX is performed in order to adopt the most efficient prediction method in terms of accuracy and computation time in the proposed strategy.

The grid-search approach is used to identify the best hyperparameters. For the LSTM model, the different ranges of hyperparameters to be optimized are as follows: epochs are set between 10 and 100, the learning rate is set as [0.5, 0.1, 0.01, 0.001, and 0.0001], and the number of hidden layer is set between 1 and 400. For the NARX model, the hyperparameter ranges for input delay, feedback delay, hidden layer size, and training function are set as [2, 5 and 20], [2, 5 and 10], between 1 and 133, and [''trainlm'', ''trainbr'', ''traind''].

B. DETERMINATION OF ENERGY RECOVERY MAXIMIZATION RATE

As previously mentioned, the power during braking varies from one driver to another because the regeneration limit is affected by the driver's acceleration behavior. A very low acceleration leads to the rotational speed being in the region of low-speed power dissipation, as presented in Fig. 2. Therefore, the strategy plans for long-term deceleration and the trigger of Freewheel mode. To determine The limits of torque and force in the wheel, a precise estimation of power flow parameters has been suggested in this work. The Power flow parameters, η_{Ba}, η_{Mi}, η_{Tr}, represent the battery efficiency during the charging or discharging, the traction inverter efficiency, and the driveline efficiency, respectively.

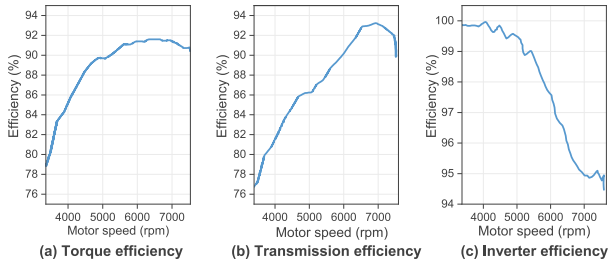

FIGURE 4. Efficiency curves for inverter electrical device and efficiency factor of PMSM Kia soul.

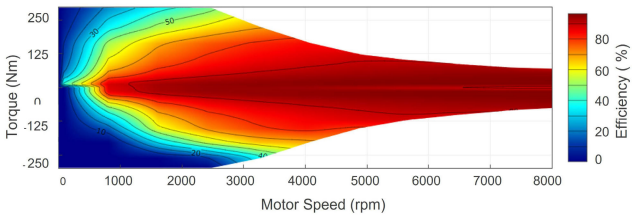

FIGURE 5. The efficiency factor of PMSM Kia soul.

The parameters of the power flow of the EV Kia Soul 2017 are studied in [52]. The reported analysis results are shown in Fig.4, demonstrating that the inverter has a maximum efficiency of 99% at low speed and a minimum efficiency of 94% at high speed. The gearbox of the Kia Soul is constant and equal to 8.206. The power regenerated in the wheel can be expressed by:

$$P_{w\_\text{pred}} = \eta_{Ba} \cdot \eta_{Mi} \cdot \eta_{Tr} \cdot P_{b\_\text{pred}} \tag{21}$$

Since ω_b is predicted, and by applying the formulas expressed in (12),(13),(14) and (18), ω_{w_pred} can be determined. Moreover, T_w is obtained using motor-battery efficiency map of Kia soul shown in Fig.5. Accordingly, the in-wheel force limit F_{lmt} and the force regenerated by the driver F_{rgn_pred} can be predicted and compared. The difference between these two parameters is used to update the horizon of the deceleration planning, as discussed in the subsequent section. Fig.6 demonstrates the driver's naturalistic behavior speed profile and the deceleration profile optimized by the proposed AEDPS. In the case of naturalistic driving maneuvers, ΔF_{nat}, which is the force difference between the motor force in traction $F_{\text{Rgn/nat}}$ and the powertrain regeneration force limit $F_{Lmt/nat}$ at a specific rotational speed ω_{nat}, defines the regeneration performance of the hlpowertrain. It should be noted that ΔF_{nat} depends on the driving style and route segment features. The maximum regeneration $F_{\text{Rgn/max}}$ and the maximum regeneration limit $F_{\text{Lmt/max}}$ for each driver's behavior are closely related to the maximum rotational speed in acceleration mode $\omega_{\max}$. $F_{\text{Rgn/max}}$ is equivalent to the optimal regenerative force that the AEDPS strategy achieves. Assumption: The Strategy assumes that $F_{\text{Rgn/max}}$ is equal to $F_{\text{Rgn/Lmt}}$ in the second step of the strategy.

The comparison between $F_{\text{Rgn/max}}$ and $F_{\text{Rgn/nat}}$ allows predicting the maximum regeneration efficiency and

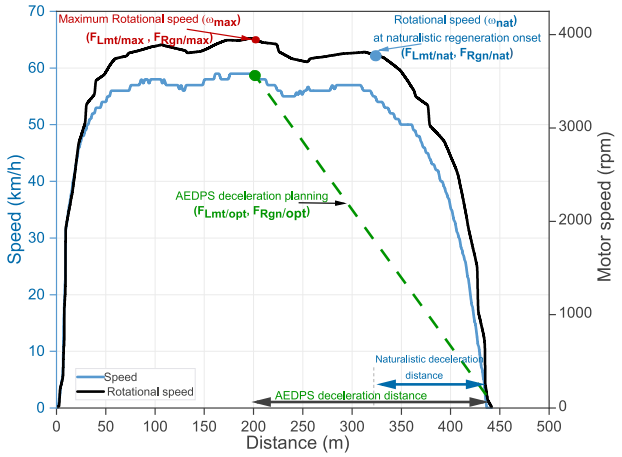

FIGURE 6. AEDPS parameters.

determining the energy recovery maximization rate expressed by $\Delta F = F_{\text{Rgn/max}} - F_{\text{Rgn/nat}}$. Depending on the resulting value of ΔF, AEDPS chooses the deceleration planning horizon when ΔF is not zero. Otherwise (if it is zero), the driver's behavior is considered optimal.

C. ADAPTATIVE OPTIMAL DECELERATION PLANNING

As previously mentioned, the ΔF determined by the forecasting model varies widely, as energy recovery is affected by the vehicle operating environment and the driving style. To promote energy regeneration, increasing the deceleration distance is essential, but it is limited by ΔF. Therefore, the optimization strategy consists of three different deceleration planning horizons; long, medium, and short. Each horizon is associated with a range of ΔF. The allocation of the deceleration horizon is done as follows:
Optimal: O N $\leq \Delta F \leq 100$ N
Short: 100 N $< \Delta F \leq 500$ N
Medium: 500 N $< \Delta F \leq 1000$ N
Long: $\Delta F > 1000$ N
As shown in Fig.2, the horizon is defined based on ΔF, and the choice of the planning horizon as input in the optimization helps to make the regenerative braking strategy adaptive. AEDPS optimizes the energy recovery performance of the powertrains by determining the optimal regeneration force that minimizes ΔF. In general, acceleration is determined by the driver, and deceleration is performed automatically by AEDPS based on the principle of an adapted optimal deceleration profile. Fig. 7 shows an example of AEDPS optimized deceleration profile at different horizons. The distance between $\omega_{\max}$ and ω_{nat} is calculated and labeled as D_{diff}. The long horizon adds all the distance D_{diff} to the naturalistic deceleration distance. The Medium horizon adds $\frac{2}{3}$ of D_{diff} to the naturalistic deceleration distance. The short horizon adds $\frac{1}{3}$ of D_{diff} to the naturalistic deceleration distance. The deceleration profile is constrained between the driving speed and the final speed at the stop position. The speed constraints in (2) must be dynamically updated to find

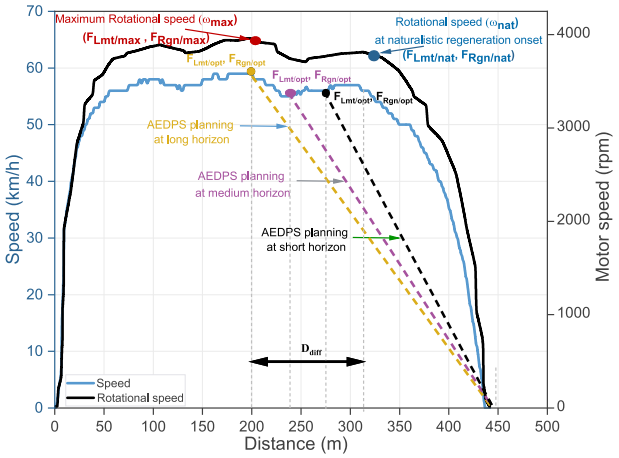

FIGURE 7. Illustrating AEDPS optimized deceleration profile at different horizons.

a set of practically feasible speed candidates at a computation node, considering the deceleration induced by the road load force, the smooth deceleration for driving preference, and the remaining deceleration distance. For different driving environments and situations, the speed constraints change as the road load forces change. To achieve speed planning that maximizes energy recuperation, an optimization problem using DP has been formulated.

1) ENERGY OPTIMIZATION BY DYNAMIC PROGRAMMING

In the proposed strategy, the dynamic programming method is employed to optimize the deceleration profile. The DP method incorporates the environmental conditions of EVs operation, including the slope and deceleration ranges of a real vehicle. Assume the deceleration started at vehicle position X_k and finished at position X_N. For any position X_i ($k \leq i \leq N$), given the speed at the road grade (or slope), θ_i is known. Assume that at X_i, the vehicle longitudinal speed and acceleration are v_i, a_i. The energy E_N during the entire vehicle deceleration from X_k to X_N is given by:

$$E_N = E_k + \sum_{i=k+1}^{N} F_{Rgn}\left(v_i, a_i, \theta_i\right) \Delta X \tag{22}$$

where E_k is the vehicle kinetic energy at X_k; $F_{Rgn}\left(v_i, a_i, \theta_i\right)$ represents the regenerative force profile from X_k to $X_N \cdot \Delta X = X_{i+1} - X_i$. The optimization problem can be formulated as follows:

Given X_k and X_N, find the sequence of a_i so that E_N is minimized and the following constraints:

$$F_{Rgn}\left(v_i, a_i, \theta_i\right) = Ma_i + \frac{1}{2}\rho A C_v v_i^2 + Mg\left(\mu \cos\left(\theta_i\right) + \sin\left(\theta_i\right)\right) \tag{23}$$

$$a_{\min} \leq a_i \leq a_{\max} \tag{24}$$

So the optimal energy during the deceleration is:

$$E_N^* = \min_{a_i}\left[E_k + \sum_{i=k+1}^{N} F_{Rgn}\left(v_i, a_i, \theta_i\right) \Delta X\right] \tag{25}$$

Using DP, the optimal sequence $\{a^*\} = \{a_i, k+1 \leq i \leq N\}$ is given by:

$$\{a^*\} = \arg\min_{a_i}\left[E_k + \sum_{i=k+1}^{N} F_{Rgn}\left(v_i, a_i, \theta_i\right) \Delta X\right] \tag{26}$$

Knowing a^*, the optimal deceleration speed profile is given the integral of $\{a^*\}$.

IV. EXPERIMENTAL RESULTS, ANALYSIS AND COMPARATIVE STUDY

This section begins with the analysis and comparison of the results of the power prediction framework using NARX and LSTM models. Subsequently, the performance of the proposed AEDPS strategy is studied in detail. Three different driving behaviors are considered, and the drivers were given several stop conditions to gain a realistic perception of the performance of the proposed AEDPS.

A. VALIDATION AND RESULT OF TIME-SERIE MODEL

Both proposed prediction models, NARX and LSTM, undergo the same training process: 80% of the data is used for training and validation, while the remaining data is reserved for testing the model. Each driver's dataset consists of 3400 cases. Before training, validating, and testing, the data is normalized using the Matlab Min-Max method. Since the cross-validation technique removes the time-dependent nature of the data, it has not been included in any of the models.

The LSTM network is configured with 100 epochs, 300 hidden layers, and a learning rate of 0.001. This initial setup results in a reasonable computation time of 169 seconds and a satisfactory RMSE of 0.91 kW. To further improve prediction accuracy, an additional fully connected layer characterized by a drop-out layer with a percentage of 0.5 and an output size of 30 is integrated into the network. This refinement significantly enhances prediction accuracy, reducing the RMSE to 0.463 kW but increasing the computation time to 1865.4 seconds. To demonstrate the model's capacity to avoid overfitting, a comparison of test and validation RMSEs is performed. The test RMSE of 0.499 kW shows that the model is not overfitting, as it closely aligns with the validation set's RMSE, with only a slight difference of 0.02. An example of predicting regenerated power by the LSTM approach for a single braking scenario is shown in Fig. 8, indicating reasonable predictions even 30 seconds in advance. Furthermore, Fig. 8 displays how the LSTM approach fits the test data and closely tracks power variation in all segments. However, the LSTM approach has a significant drawback in terms of computational time, which is considerably high. In light of this, the data is re-evaluated using the NARX model due to its

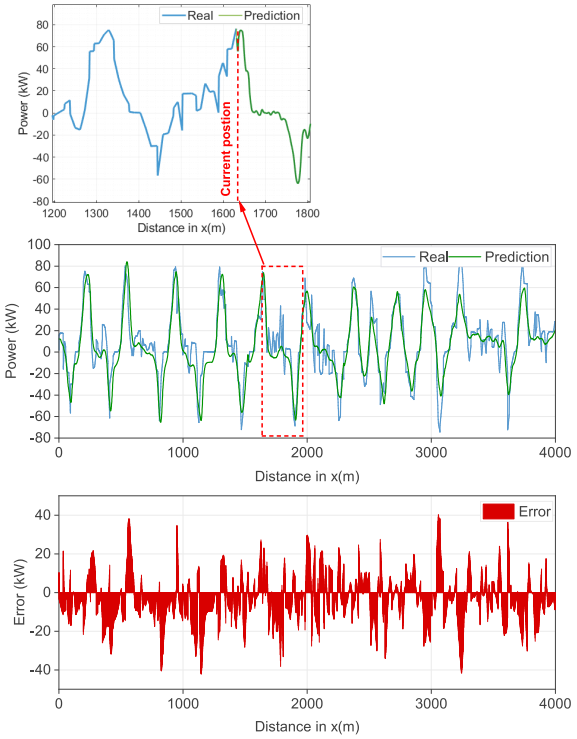

FIGURE 8. Forecast results of 12 segments for the proposed NARX model.

lower computational power and faster training time. Through grid search hyperparameter optimization, the best NARX structure is identified with 75 hidden layers, 2 input delays, 2 feedback delays, and trainlm as the best training function. This configuration significantly reduces the computational time to 8.841 seconds, while achieving an optimal RMSE similar to LSTM, at 0.4402 kW. As a result of these findings, NARX seems to be a better choice for predicting efficiency in terms of computational time.

B. AEDPS POWERTRAIN'S REGENERATION PERFORMANCE ANALYSIS

To evaluate the effectiveness of AEDPS, which is based on adaptive deceleration planning, and to assess the resulting powertrain regeneration performance, the amount of energy regenerated for different deceleration horizons adapted to the driving style is analyzed. Three naturalistic driving behaviors with average maximum speeds of 54 km/h, 47 km/h, and 63 km/h under 5 stopping segments are chosen to represent the driver's maximum speed preferences and variable braking behaviors. The segments are selected to include combinations of downhill slopes, high downhill slopes, and flat downhill slopes, resulting in a total of 15 different scenarios as shown in Table 3. However, uphill slope sections are not studied in this article due to their limited potential for energy-maximizing regeneration. For each AEDPS driver model, the adapted horizon (long, medium, and short) is automatically integrated for each driving scenario, as explained in Fig.7. The optimal regeneration force of AEDPS, $F_{\mathrm{Rgn/opt}}$ is calculated using an electric vehicle model composed of maximized

TABLE 3. Summary of AEDPS predicted key parameters of the different driving styles.

Parameter/ Name	Driver/ Seg	1st	2ed	3rd	4th	5th
Slope	1/2/3	Downhill	Downhill	Flat	Downhill	Flat
3* $\omega_{\max}$(Rpm)	1	-3975	-3693	-3900	-3510	-3769
	2	-3319	-3116	-3100	-3300	-3262
	3	-4783	-4613	-5000	-4569	-4585
3*$v_{\max}$ (km/h)	1	59	55	59	54	56
	2	50	48	57	50	48
	3	72	65	76	68	68
3*$\mathbf{T}_{\mathrm{Lmt/\,max}}$(Nm)	1	-128	-114	-122	-110	-118
	2	-63.8	-60	-57	-63	-59
	3	-169	-160	-175	-158	-156
3*$\mathbf{F}_{\mathrm{Lmt/\,max}}$(N)	1	-3498	-3116	-3334	-2900	-3225
	2	-1743	-1587	-1650	-1749	-1612
	3	-4634	-4232	-4783	-4318	-4264
3*$\mathbf{F}_{\mathrm{Rgn}/opt}$(N)	1	-3225	-3116	-2210	-2811	-2830
	2	-1743	-1504	-1352	-1749	-1369
	3	-4573	-4174	-3340	-4241	-3070
3*$\mathbf{F}_{\mathrm{Rgn}/nat}$(N)	1	-1559	-3116	-384	-2119	-505
	2	-1743	-1405	-1263	-557	-1267
	3	-3745	-4116	-2750	-1061	-1810
3*ΔF(N)	1	-1939	0	-2950	-781	-2719
	2	0	-99	-387	-1192	-345
	3	-889	-58	-2033	-3257	-2454
3*Horizon	1	Long	Optimal	Long	Medium	Long
	2	Optimal	Optimal	Short	Long	Short
	3	Medium	Optimal	Long	Long	Long
3*$\mathbf{DFR}_{\mathrm{AEDPS}}$(%)	1	92	100	66	96	87
	2	100	93	81	100	84
	3	98	98	69	98	72
3*$\mathbf{AEDPS}_{\mathrm{Dec}/dis}$(m)	1	214	61	185	183	257
	2	58	63	132	187	85
	3	161	67	198	253	280
3*$\mathbf{Driver}_{\mathrm{Dec}/dis}$(m)	1	146	61	124	169	89
	2	58	83	100	85	85
	3	96	67	74	106	45
3* AEDPS regeneration efficiency improvement %	1	48	0	55	23	72
	2	0	0	5	69	6
	3	18	0	12	73	29

power regeneration and optimized vehicle speed. To ensure a fair comparison, the results of the forces regenerated by human drivers, $F_{\mathrm{Rgn/Nat}}$, are also calculated using the predicted power and rotational speed of driver behavior. Fig.9 and Fig.10 illustrate the regeneration forces of AEDPS and of the driver in 6 scenarios, with the deceleration horizon adapted to each naturalistic regeneration performance. The differences in deceleration starting points result in a significant difference in regenerative forces between AEDPS and human drivers. As the deceleration points approach, optimal velocity generates maximum regeneration force, as shown by the green lines, pushing the motor regeneration to its physical limit (red line). This indicates that the deceleration profiles of AEDPS increase the amount of regenerated energy compared to the driver regeneration force (blue line). Furthermore, the driver behavior (Table 3) show shorter deceleration distance values than ADPES, resulting in lower energy recovery. Except for driver 2 in segment 1 and the three drivers in segment 2, who are predicted with optimal braking behaviors, the distance is doubled or even tripled. This means that a short deceleration distance, compared to the AEDPS-optimized deceleration distance, reduces the possibility of energy recovery.

The proposed strategy employs a prediction model for long-horizon (30 seconds) power forecast, primarily focusing on predicting ΔF for each scenario. ΔF represents the energy recovery maximization rate, which is used to make the deceleration planning adaptive by selecting the best

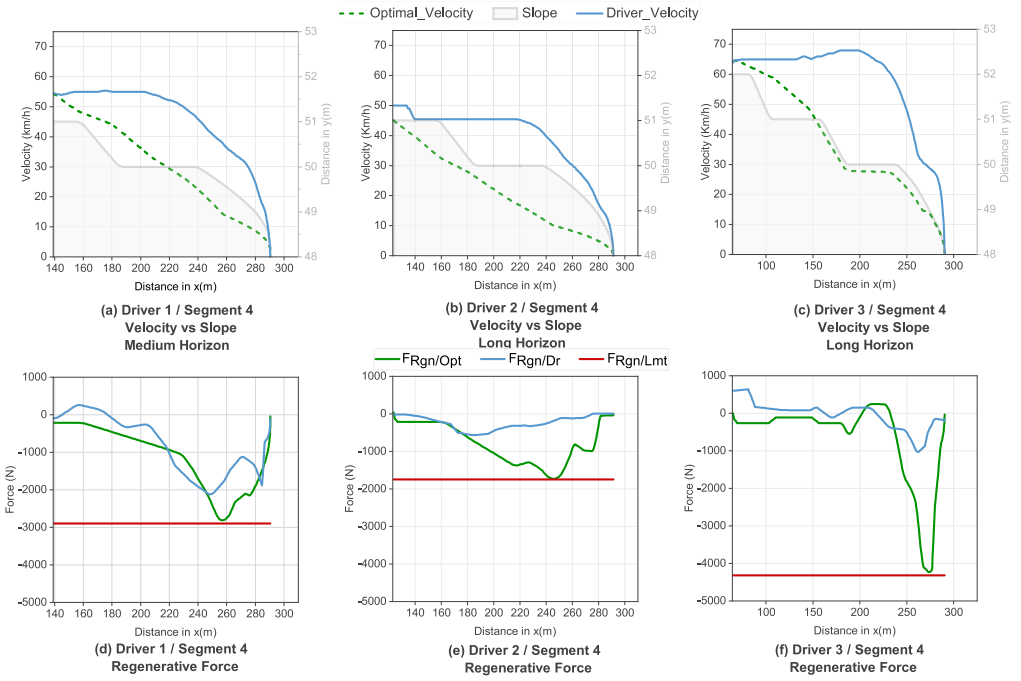

FIGURE 9. Adaptative regeneration maximization by AEDPS in downhill slope roads.

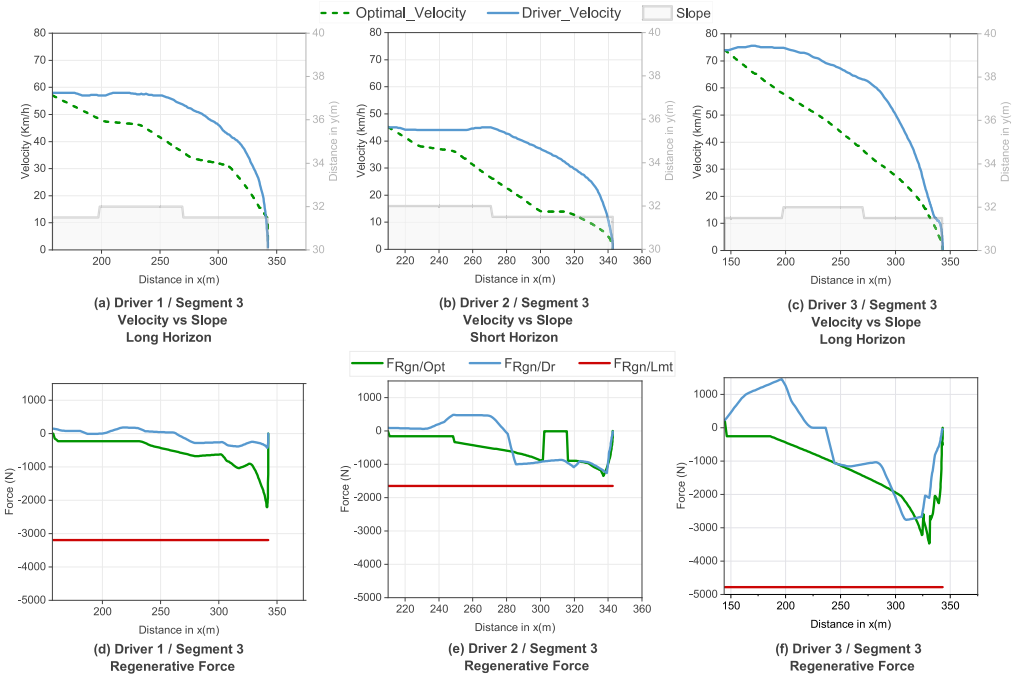

FIGURE 10. Adaptative regeneration maximization by AEDPS in flat slope roads.

horizon. Furthermore, reducing vehicle speed by initiating deceleration at the selected horizon allows the potential for maximizing regeneration up to the physical limits of an electrified powertrain; however, not all the energy recovery maximization rate can be regenerated. As a result, AEDPS produces the optimal deceleration profiles based on regeneration limitations and road topology to minimize the value of ΔF up to $\Delta F_{\text{opt}} = F_{\text{Lmt / max}} - F_{\text{Rgn /opt}}$. The comparison of ΔF_{opt} in the two types of road slopes, medium downhill slope in Fig.9, and nearly flat slope in Fig.10, is the second criterion for evaluating AEDPS energy regeneration performance. Fig.9 displays the segment with a medium downhill road slope corresponding to segment 4. Fig.9 (a) demonstrates that the case of significant deceleration with a downhill slope road results in a considerable transitory regeneration force, as shown in Fig.9 (d). This is not valid for a significant deceleration with a constant value of road slope and for a cruise mode with a downhill slope road, which results in low

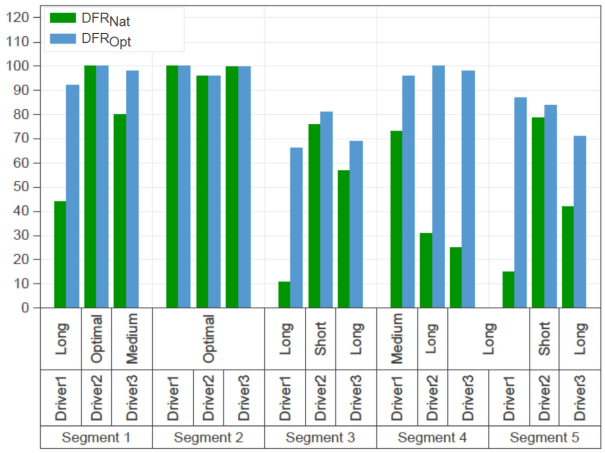

FIGURE 11. Comparaison between DFR of naturalistic speed behaviors and DFR of AEDPS speed profile of each driver during five segments.

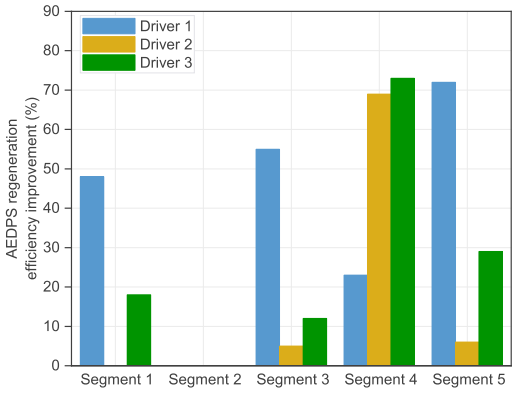

FIGURE 12. Indicator of regeneration efficiency improvement of each driver during five segments.

demand for transitory regeneration force. Fig.9 shows that the optimal regeneration force converges toward the maximum regeneration force until it reaches the force $F_{\mathrm{Lmt/max}}$ (red line), which imposes ΔF_{opt} to be zero. This convergence results from the various horizons assigned to each driver: medium for driver 1, long for driver 2, and long for driver 3. However, as shown in Fig.10, which shows segment 3 with a flat road, the planned deceleration profiles minimize ΔF but do not reach a zero value for ΔF_{opt} , even with a long horizon. This is primarily due to the effect of road load forces on regeneration performance. In fact, road load forces decrease on down-hill roads, leading to the enhancement of energy recovery. Flat roads' load forces increase slightly as only regenerative force is required for deceleration. As a result, the trend of $F_{\mathrm{Rgn\ /\ Opt}}$ convergence on the two road slopes proves that the strategy satisfies the consideration of road loads and confirms its ability to follow the regeneration limit.

A third relevant analysis is to validate the adaptation of regeneration efficiency improvements to each naturalistic regeneration performance. A strategy simulation is applied to all the route's deceleration events for each of the three driving behaviors. During each scenario, the deceleration force ratio (DFR) is presented in Fig.11. DFR is the ratio between the physical limits of an electrified powertrain and the regeneration force for the current EV's speed. Fig. 11 shows the difference between DFR of AEDPS speed profile (DFR_{Opt}) and DFR of naturalistic speed behavior (DFR_{Dr}). Furthermore, the deceleration planning horizon is presented in the same figure, showing that it is adapted to naturalistic regeneration performance. A performance indicator of regeneration efficiency improvement is calculated by subtracting $DFR_{\mathrm{opt}} - DFR_{\mathrm{nat}}$, and presented in Fig.12. This figure depicts the gain, which varies dynamically from one scenario to another. The energy recovery performance of Driver 1 improves by 48% over a long horizon in segment 1, 0% over an optimal horizon in segment 2, 55% over a long horizon in segment 3, 23% over a medium horizon in segment 4, and 72% over a long horizon in segment 5. This trend indicates that the adaptive aspect of regeneration performance enhancement is adequate, as ensured by the deceleration planning horizon dynamics, and it is significantly affected by road topology. Furthermore, segment 2 has a very high downhill slope compared to other segments. Table 3 presents the naturalistic regeneration performance for the three drivers predicted as optimal in segment 2. This makes an additional claim about how the driver's regeneration performance varies depending on the road topology and the importance of creating an adaptive regenerative braking strategy. The maximum improvement in the regeneration of each driver does exceed 60%, and it is not achieved in the same segment, as shown in Fig.12. Driver 1 has improved regeneration up to 72% in segment 5, driver 2 up to 69% in segment 4, and driver 3 up to 73% in segment 4. Furthermore, the regeneration efficiency improvement rate shows a potential increase in energy recovery performance of 0%, 0%, 5%, 69%, and 6% for the five road segments, respectively. This increase in performance is more significant in the case of driver 1 (48%, 0%, 55%, 23%, and 72%) and driver 3 (18%, 0%, 12%, 73%, and 29%), characterized by a high driving speed, leading to a higher regeneration limit of the powertrain, and a short deceleration distance, allowing maximization of the regeneration distance. Therefore, the improvement rate clearly demonstrates that it is not only related to road topology but also to driver acceleration and braking behaviors. In the end, these previous results prove that the proposed strategy improves the acceptance of the braking control strategy by adapting deceleration planning to the regeneration performance of drivers in each scenario.

Several authors also use the speed-acceleration probability distribution (SAPD) as an alternative to reflect the dynamics of driving behavior. Fig. 13 and Fig. 14 below depicts the SAPD for the naturalist driver data as well as the output from the proposed approach, respectively. This figure shows that SAPD creates velocity-acceleration groups and gives $V_{in} = 2$ km/h and $a_{in} = 0.5$ m/s^2 as velocity and acceleration interval lengths, respectively. Furthermore, in an urban context, driving data is typically separated into four phases: stopping,

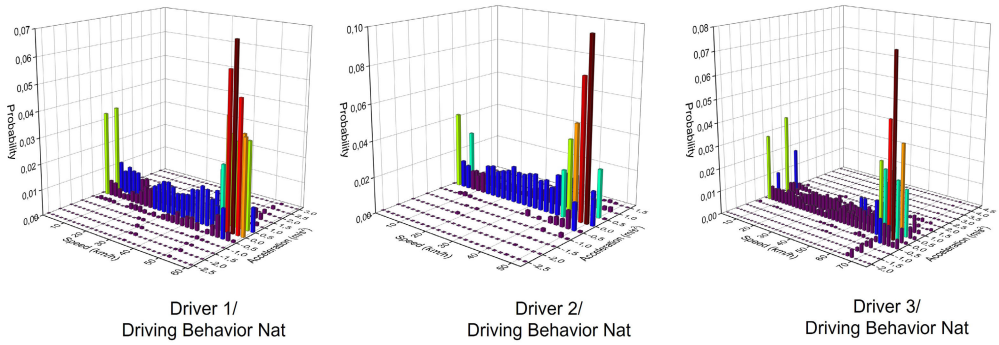

FIGURE 13. The SAPD of the naturalistic driving behaviors.

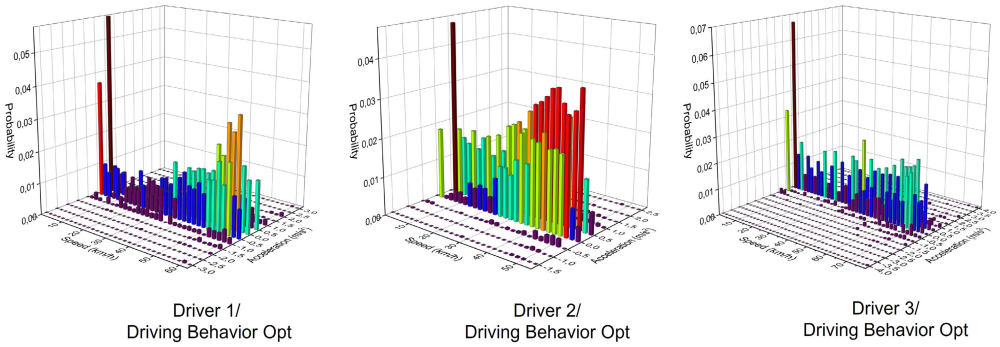

FIGURE 14. The SAPD of the optimal behaviors.

accelerating, deceleration, and cruising

$$\begin{cases} v = 0 \text{ AND abs } (a) \leq 0.15, & \text{stopping} \\ v > 0 \text{ AND abs } (a) \leq 0.15. & \text{cruising} \\ v > 0 \text{ AND } a > 0.15, & \text{accelerating} \\ v > 0 \text{ AND } a < -0.15, & \text{decelerating} \end{cases} \tag{27}$$

At first, the SAPD illustrated in Fig. 13 demonstrates that the speed-acceleration probability distributions of the naturalistic driving behavior data for the three drivers exhibit both similar and distinct characteristics. Driver 3 has the greatest permitted maximum speed of 75 km/h, while Driver 1 has a maximum speed of 60 km/h, and Driver 2 has a maximum speed of 50 km/h. In terms of similarities among the three drivers, the distribution probability of the Cruise phase, as defined previously, is more concentrated in the maximum speed, and presents the highest probability (Probability>0.6%) compared to other driving phases. The probability distribution of the stopping phase also exhibits a significant average density (Probability>0.3%) for all three drivers. Additionally, the deceleration phase has a Medium probability and is also more concentrated in the maximum speed. Secondly, the SAPD illustrated in Fig. 14 demonstrates the velocity-acceleration probability distributions of the optimal behaviors of the three drivers. This figure shows that the three drivers maintain the same maximum speed as in their naturalistic behavior. Furthermore, the probability distribution of the stopping phase also maintains a significant average density. However, the probability distribution of the Cruise and deceleration phases has become much less concentrated on the maximum speed and more distributed over different speed values. This confirms the experimental context of the real data and also validates the effectiveness of the suggested approach in generating the optimal behavior.

C. COMPARATIVE STUDY

The Previous work has predominantly focused on long-term deceleration planning over a residual distance of 200 meters, with the horizon determined by the vehicle's installed sensor [40]. These strategies have proven effective for driving behaviors characterized by a uniform maximum speed (90 km/h) and under specific experimental conditions. The results of these studies reveal that long-term planning yields substantial benefits, with minor variance amongst ten drivers, ranging between 41% and 51%. However, these approaches only consider the long-term speed profile for driving behaviors with a maximum cruise speed of (90 km/h) and fail to account for variations in energy regeneration performance for other driving behaviors with differing maximum speed preferences and driving conditions. Our proposed strategy addresses these shortcomings by examining the driving behaviors of three drivers with different maximum speed preferences and various slope levels. This approach

illuminates how these factors influence the variability of naturalistic regeneration performance. Compared to other strategies, the proposed strategy is uniquely capable of predicting naturalistic regeneration performance in each stopping environment. The prediction of these performances has been shown to be especially beneficial in numerous instances where naturalistic deceleration behavior is optimal and assistance is considered useless, thereby helping to limit driver disruption from irrelevant advice or warnings. Moreover, our strategy adjusts the deceleration horizon using three distinct horizons–long, medium, and short–rendering the approach adaptive and reducing the computational load required to generate an optimal speed profile in real-time. Consequently, as our proposed strategy adapts to naturalistic regeneration performance for drivers with varying maximum speed preferences, the improvement in regeneration performance varied significantly from one driving behavior to another and from one scenario to another.

V. CONCLUSION

This paper presents the design of an adaptive braking strategy based on naturalistic regeneration performance for an electric vehicle. Using NARX methods, the proposed AEDPS predicts the power with long-horizon forecasting (30 seconds), allowing anticipation of the difference between naturalistic energy regeneration and the physical limits of an electrified powertrain corresponding to maximum speed preference. This previous step allows evaluation of the naturalistic regeneration performance, which makes the deceleration planning horizon adapted to this performance. AEDPS considers three deceleration planning horizons: long, medium, and short. The long horizon improves energy regeneration for the driver with low naturalistic regeneration performance by developing long deceleration profiles, while medium and short horizons are assigned to moderate and minimal naturalistic regeneration performance scenarios, respectively. AEDPS uses DP to implement the deceleration profile that maximizes energy recovery. Implementing the adaptive control strategy resulted in a prediction of optimal naturalistic regeneration behavior in segment 2 for the three drivers, limiting irrelevant warnings and increasing the eco-feedback technology's effectiveness. The obtained results through simulations of the AEDPS strategy by three drivers that have different preferences for maximum speed when driving between two-stop events are promising. It can maximize energy regeneration up to the individual physical limits of an electrified powertrain on downhill roads and 10-20% less on flat roads. This result proves that the strategy satisfies the consideration of road loads and confirms its ability to reach optimal regeneration performance, satisfying maximum speed preference. Developing appropriate strategies for drivers' preferences improves the control strategy's acceptability and efficiency. Furthermore, the result shows 39,6% improvement in regeneration efficiency for driver 1, 16% for driver 2, and 26% for driver 3, and forecasting the optimality of some deceleration behaviors. This trend proves that the adaptive strategy effectively manages the individual maximization of regeneration and improves the energy efficiency of EVs. Therefore, the proposed AEDPS exhibits several notable advantages. It significantly reduces energy consumption by maximizing regeneration to the physical limits of an electrified powertrain and considering driver behavior preference. Moreover, it enhances driver acceptance of the braking control strategy by adapting the deceleration planning horizon to naturalistic regeneration performance and improving eco-feedback technology's effectiveness by minimizing unnecessary alerts. This adaptive braking control strategy also motivates the driver to adopt AEDPS by demonstrating the gain it can bring compared to its naturalistic behaviors. Additionally, this strategy mitigates the computational burden required to generate an optimal velocity profile in real-time, by avoiding extra calculations for short-horizon deceleration planning and optimal naturalistic deceleration behavior.

The work presented in this manuscript lays the basis for designing an adaptive AEDPS for electric vehicles, considering static road information such as road grades and stop signs detected by intelligent cameras. In the future, enhanced connectivity with other vehicles and infrastructure may enable the following:

(1) Expanding to encompass other dynamic deceleration conditions, such as car-following situations, and offering adaptive deceleration planning to accommodate driver behaviors under these circumstances. The model of power regeneration forecasting should integrate relative velocity, relative distance, and the speed of the ego vehicle.

(2) Maximizing the benefits of AEDPS, adaptive deceleration planning should generate optimal deceleration in more complex traffic scenarios, including signalized intersections. The proposed strategy could utilize SPAT information from an actual signal controller operation to guide the driver through signalized intersections, thus maximizing regeneration and adapting the assistance according to their regenerative performance.

(3) Integrating steering angle and yaw moment distribution to amplify the effectiveness of regenerative braking by AEDPS in scenarios such as decelerating before signal signs, at the same time changing lanes to the right or left.

(4) While this paper proposes an AEDP for current energy systems considering the optimal operating temperature range for lithium-ion batteries (typically 15 to 35 °C), it doesn't address the battery's charge capacity at very low temperatures (between −20 and −40 °C). This is crucial to ensure the strategy's effectiveness in colder countries such as Canada and Sweden.

(5) In adverse weather conditions such as rain, snow, or icy roads, drivers tend to be more careful, and decelerate earlier and exhibit reduced vehicle speed, acceleration, and deceleration rates. Winter road conditions are also more likely to be slippery, causing additional loss of regenerated energy during braking. Therefore, AEDPS should factor in the impact of weather on naturalistic regenerative performance, enhancing its robustness under such conditions.

(6) The proposed AEDPS implementation holds significant promise for electric buses, which have relatively fixed routes and must stop at inter-route stations for passenger pick-up/drop-off. The total mass, a fundamental parameter of the longitudinal dynamic model and energy regeneration (particularly in downhill movement scenarios), changes as passengers board and disembark at bus stations. This key characteristic should be addressed within the context of eco-friendly braking assistance for electric buses.

ACKNOWLEDGMENT

The authors would like to thank the Foundation of Université du Québec à Trois-Rivières, Canada Research Chair Program; Natural Sciences and Engineering Research Council of Canada. They also like to thank Mohsen Kandidayeni for his valuable suggestions to improve the quality of the paper.

REFERENCES

[1] W. R. Black and N. Sato, "From global warming to sustainable transport 1989–2006," *Int. J. Sustain. Transp.*, vol. 1, no. 2, pp. 73–89, May 2007.
[2] S. Perveen, T. Yigitcanlar, M. Kamruzzaman, and D. Agdas, "How can transport impacts of urban growth be modelled? An approach to consider spatial and temporal scales," *Sustain. Cities Soc.*, vol. 55, Apr. 2020, Art. no. 102031.
[3] M. Lombardi, K. Panerali, S. Rousselet, and J. Scalise. (2018). *Electric Vehicles for Smarter Cities: The Future of Energy and Mobility*. World Economic Forum. [Online]. Available: http://www3.weforum.org/docs/WEF_2018_%20Electric_For_Smarter_Cities.pdf
[4] S. Hima, S. Glaser, A. Chaibet, and B. Vanholme, "Controller design for trajectory tracking of autonomous passenger vehicles," in *Proc. 14th Int. IEEE Conf. Intell. Transp. Syst. (ITSC)*, Oct. 2011, pp. 1459–1464.
[5] G. Li, D. Wu, J. Hu, Y. Li, M. S. Hossain, and A. Ghoneim, "HELOS: Heterogeneous load scheduling for electric vehicle-integrated microgrids," *IEEE Trans. Veh. Technol.*, vol. 66, no. 7, pp. 5785–5796, Jul. 2017.
[6] H. Vdovic, J. Babic, and V. Podobnik, "Automotive software in connected and autonomous electric vehicles: A review," *IEEE Access*, vol. 7, pp. 166365–166379, 2019.
[7] Q. Jin, G. Wu, K. Boriboonsomsin, and M. J. Barth, "Power-based optimal longitudinal control for a connected eco-driving system," *IEEE Trans. Intell. Transp. Syst.*, vol. 17, no. 10, pp. 2900–2910, Oct. 2016.
[8] F. Mensing, E. Bideaux, R. Trigui, and H. Tattegrain, "Trajectory optimization for eco-driving taking into account traffic constraints," *Transp. Res. D, Transp. Environ.*, vol. 18, pp. 55–61, Jan. 2013.
[9] A. Sciarretta, G. D. Nunzio, and L. L. Ojeda, "Optimal ecodriving control: Energy-efficient driving of road vehicles as an optimal control problem," *IEEE Control Syst. Mag.*, vol. 35, no. 5, pp. 71–90, Oct. 2015.
[10] S. Wang and X. Lin, "Eco-driving control of connected and automated hybrid vehicles in mixed driving scenarios," *Appl. Energy*, vol. 271, Aug. 2020, Art. no. 115233.
[11] J. Han, A. Vahidi, and A. Sciarretta, "Fundamentals of energy efficient driving for combustion engine and electric vehicles: An optimal control perspective," *Automatica*, vol. 103, pp. 558–572, May 2019.
[12] M. Li, X. Wu, X. He, G. Yu, and Y. Wang, "An eco-driving system for electric vehicles with signal control under V2X environment," *Transp. Res. C, Emerg. Technol.*, vol. 93, pp. 335–350, Aug. 2018.
[13] F. Golbabaei, T. Yigitcanlar, A. Paz, and J. Bunker, "Individual predictors of autonomous vehicle public acceptance and intention to use: A systematic review of the literature," *J. Open Innov., Technol., Market, Complex.*, vol. 6, no. 4, p. 106, Dec. 2020.
[14] R. A. Dollar and A. Vahidi, "Efficient and collision-free anticipative cruise control in randomly mixed strings," *IEEE Trans. Intell. Vehicles*, vol. 3, no. 4, pp. 439–452, Dec. 2018.
[15] S. E. Li, S. Xu, X. Huang, B. Cheng, and H. Peng, "Eco-departure of connected vehicles with V2X communication at signalized intersections," *IEEE Trans. Veh. Technol.*, vol. 64, no. 12, pp. 5439–5449, Dec. 2015.
[16] L. Hu, Y. Zhong, W. Hao, B. Moghimi, J. Huang, X. Zhang, and R. Du, "Optimal route algorithm considering traffic light and energy consumption," *IEEE Access*, vol. 6, pp. 59695–59704, 2018.
[17] J. Han, A. Sciarretta, L. L. Ojeda, G. De Nunzio, and L. Thibault, "Safe- and eco-driving control for connected and automated electric vehicles using analytical state-constrained optimal solution," *IEEE Trans. Intell. Vehicles*, vol. 3, no. 2, pp. 163–172, Jun. 2018.
[18] Z. Yang, Y. Feng, X. Gong, D. Zhao, and J. Sun, "Eco-trajectory planning with consideration of queue along congested corridor for hybrid electric vehicles," *Transp. Res. Rec., J. Transp. Res. Board*, vol. 2673, no. 9, pp. 277–286, Sep. 2019.
[19] W. Zhao, D. Ngoduy, S. Shepherd, R. Liu, and M. Papageorgiou, "A platoon based cooperative eco-driving model for mixed automated and human-driven vehicles at a signalised intersection," *Transp. Res. C, Emerg. Technol.*, vol. 95, pp. 802–821, Oct. 2018.
[20] F. Wang and B. Zhuo, "Regenerative braking strategy for hybrid electric vehicles based on regenerative torque optimization control," *Proc. Inst. Mech. Eng., D, J. Automobile Eng.*, vol. 222, no. 4, pp. 499–513, Apr. 2008.
[21] H. Liu, Y. Lei, Y. Fu, and X. Li, "An optimal slip ratio-based revised regenerative braking control strategy of range-extended electric vehicle," *Energies*, vol. 13, no. 6, p. 1526, Mar. 2020.
[22] C. Qiu, G. Wang, M. Meng, and Y. Shen, "A novel control strategy of regenerative braking system for electric vehicles under safety critical driving situations," *Energy*, vol. 149, pp. 329–340, Apr. 2018.
[23] S. Liu, Z. Li, H. Ji, Z. Hou, and L. Fan, "A novel electric vehicle braking energy recovery method based on model free adaptive control algorithm with input and output constraints," in *Proc. IEEE 10th Data Driven Control Learn. Syst. Conf. (DDCLS)*, May 2021, pp. 1503–1509.
[24] H. Dong, W. Zhuang, B. Chen, Y. Wang, Y. Lu, Y. Liu, L. Xu, and G. Yin, "A comparative study of energy-efficient driving strategy for connected internal combustion engine and electric vehicles at signalized intersections," *Appl. Energy*, vol. 310, Mar. 2022, Art. no. 118524.
[25] F. Sangtarash, V. Esfahanian, H. Nehzati, S. Haddadi, M. A. Bavanpour, and B. Haghpanah, "Effect of different regenerative braking strategies on braking performance and fuel economy in a hybrid electric bus employing CRUISE vehicle simulation," *SAE Int. J. Fuels Lubricants*, vol. 1, no. 1, pp. 828–837, Jun. 2008.
[26] L. Chu, F. Zhou, J. Guo, and M. Shang, "Investigation of determining of regenerative braking torque based on associated efficiency optimization of electric motor and power battery using GA," in *Proc. Int. Conf. Electron. Mech. Eng. Inf. Technol.*, vol. 6, Aug. 2011, pp. 3238–3241.
[27] K. Min, G. Sim, S. Ahn, M. Sunwoo, and K. Jo, "Vehicle deceleration prediction model to reflect individual driver characteristics by online parameter learning for autonomous regenerative braking of electric vehicles," *Sensors*, vol. 19, no. 19, p. 4171, Sep. 2019.
[28] Z. Chen, S. Wu, S. Shen, Y. Liu, F. Guo, and Y. Zhang, "Co-optimization of velocity planning and energy management for autonomous plug-in hybrid electric vehicles in urban driving scenarios," *Energy*, vol. 263, Jan. 2023, Art. no. 126060.
[29] R. Bautista-Montesano, R. Galluzzi, Z. Mo, Y. Fu, R. Bustamante-Bello, and X. Di, "Longitudinal control strategy for connected electric vehicle with regenerative braking in eco-approach and departure," *Appl. Sci.*, vol. 13, no. 8, p. 5089, Apr. 2023.
[30] C. Pan, A. Huang, J. Wang, L. Chen, J. Liang, W. Zhou, L. Wang, and J. Yang, "Energy-optimal adaptive cruise control strategy for electric vehicles based on model predictive control," *Energy*, vol. 241, Feb. 2022, Art. no. 122793.
[31] H. Wei, L. Fan, Q. Ai, W. Zhao, T. Huang, and Y. Zhang, "Optimal energy allocation strategy for electric vehicles based on the real-time model predictive control technology," *Sustain. Energy Technol. Assessments*, vol. 50, Mar. 2022, Art. no. 101797.
[32] H. Chen, L. Guo, H. Ding, Y. Li, and B. Gao, "Real-time predictive cruise control for eco-driving taking into account traffic constraints," *IEEE Trans. Intell. Transp. Syst.*, vol. 20, no. 8, pp. 2858–2868, Aug. 2019.
[33] S. Xu, X. Zhao, N. Yang, and Z. Bai, "Control strategy of braking energy recovery for range-extended electric commercial vehicles by considering braking intention recognition and electropneumatic braking compensation," *Energy Technol.*, vol. 8, no. 9, Sep. 2020, Art. no. 2000407.
[34] B. Sun, W. Deng, R. He, J. Wu, and Y. Li, "Personalized eco-driving for intelligent electric vehicles," in *Proc. Intell. Connected Vehicles Symp.*, Kunshan, China, 2018.
[35] T. Yuan, R. Liu, X. Zhao, Q. Yu, X. Zhu, and S. Wang, "Analysis of normal stopping behavior of drivers at urban intersections in China," *J. Adv. Transp.*, vol. 2022, pp. 1–17, Jul. 2022.
[36] E. Brandenburg, L. Doria, A. Gross, T. Günzler, and H. Smieszek, *Grundlagen und Anwendungen der Mensch-Maschine-Interaktion: 10. Berliner Werkstatt Mensch-Maschine-Systeme 10.–12. Oktober 2013; Proceedings. Universitätsverlag der TU Berlin*. Berlin, Germany: Universitätsverlag der TU Berlin, 2014.

[37] A. de Moura Oliveira, E. Bertoti, J. Eckert, R. Yamashita, E. dos Santos Costa, L. C. d. A. e Silva, and F. G. Dedini, "Evaluation of energy recovery potential through regenerative braking for a hybrid electric vehicle in a real urban drive scenario," SAE Tech. Paper, 2016-36-0348, 2016.
[38] Y. Xing, C. Lv, D. Cao, and C. Lu, "Energy oriented driving behavior analysis and personalized prediction of vehicle states with joint time series modeling," *Appl. Energy*, vol. 261, Mar. 2020, Art. no. 114471.
[39] M. Mohammadi, S. Heydari, P. Fajri, F. Harirchi, and Z. Yi, "Energy-aware driving profile of autonomous electric vehicles considering regenerative braking limitations," in *Proc. IEEE Transp. Electrific. Conf. Expo. (ITEC)*, Jun. 2022, pp. 196–201.
[40] D. Kim, J. S. Eo, and K. K. Kim, "Service-oriented real-time energy-optimal regenerative braking strategy for connected and autonomous electrified vehicles," *IEEE Trans. Intell. Transp. Syst.*, vol. 23, no. 8, pp. 11098–11115, Aug. 2022.
[41] D. Schwarze, M. G. Arend, and T. Franke, "The effect of displaying kinetic energy on hybrid electric vehicle drivers' evaluation of regenerative braking," in *Congress of the International Ergonomics Association*. Cham, Switzerland: Springer, 2018, pp. 727–736.
[42] S. M. Iranmanesh, H. N. Mahjoub, H. Kazemi, and Y. P. Fallah, "An adaptive forward collision warning framework design based on driver distraction," *IEEE Trans. Intell. Transp. Syst.*, vol. 19, no. 12, pp. 3925–3934, Dec. 2018.
[43] J. Fleming, X. Yan, and R. Lot, "Incorporating driver preferences into eco-driving assistance systems using optimal control," *IEEE Trans. Intell. Transp. Syst.*, vol. 22, no. 5, pp. 2913–2922, May 2021.
[44] X. Tian, Y. Cai, X. Sun, Z. Zhu, and Y. Xu, "An adaptive ECMS with driving style recognition for energy optimization of parallel hybrid electric buses," *Energy*, vol. 189, Dec. 2019, Art. no. 116151.
[45] S. Wang, P. Yu, D. Shi, C. Yu, and C. Yin, "Research on eco-driving optimization of hybrid electric vehicle queue considering the driving style," *J. Cleaner Prod.*, vol. 343, Apr. 2022, Art. no. 130985.
[46] W. Xu, H. Chen, H. Zhao, and B. Ren, "Torque optimization control for electric vehicles with four in-wheel motors equipped with regenerative braking system," *Mechatronics*, vol. 57, pp. 95–108, Feb. 2019.
[47] H. Pacejka, *Tire and Vehicle Dynamics*. Amsterdam, The Netherlands: Elsevier, 2005.
[48] Accessed: Jan. 20, 2023. [Online]. Available: https://www.septentrio.com/en/products/gnss-ins-receivers
[49] F. K. Ayevide, S. Kelouwani, A. Amamou, M. Kandidayeni, and H. Chaoui, "Estimation of a battery electric vehicle output power and remaining driving range under subfreezing conditions," *J. Energy Storage*, vol. 55, Nov. 2022, Art. no. 105554.
[50] S. Nan, R. Tu, T. Li, J. Sun, and H. Chen, "From driving behavior to energy consumption: A novel method to predict the energy consumption of electric bus," *Energy*, vol. 261, Dec. 2022, Art. no. 125188.
[51] H. Shen, X. Zhou, H. Ahn, M. Lamantia, P. Chen, and J. Wang, "Personalized velocity and energy prediction for electric vehicles with road features in consideration," *IEEE Trans. Transport. Electrific.*, p. 1, 2023, doi: 10.1109/TTE.2023.3241098.
[52] J. D. Valladolid, D. Patino, G. Gruosso, C. A. Correa-Flórez, J. Vuelvas, and F. Espinoza, "A novel energy-efficiency optimization approach based on driving patterns styles and experimental tests for electric vehicles," *Electronics*, vol. 10, no. 10, p. 1199, May 2021.

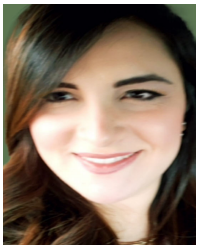

MARWA ZIADIA received the B.S. degree in computer science from the National School of Engineers of Tunis (ENSIT), Tunis, Tunisia, in 2010, the master's degree in communication and embedded computer systems security (with auditor diploma) from the Computer Science Superior Institute (ISI), Tunis, in 2012, and the master's degree in mechanical engineering from Université du Québec à Trois-Rivières (UQTR), Trois-Rivières, QC, Canada, in 2020, where she is currently pursuing the Ph.D. degree with the Department of Mechanical Engineering. Her research interests include electric vehicles, energy efficiency, intelligent transport systems, vehicle dynamics, machine learning, modeling, optimal control, and contributions to making our vehicles efficient and more eco-friendly.

SOUSSO KELOUWANI (Senior Member, IEEE) received the Ph.D. degree in robotics systems from Ecole Polytechnique de Montreal, in 2011. He completed the postdoctoral internship on fuel cell hybrid electric vehicles with Université du Québec à Trois-Rivières (UQTR), in 2012. Since 2017, he has been a Full Professor of mechatronics with the Department of Mechanical Engineering, UQTR. He holds four patents in U.S. and Canada. He has published more than 100 scientific articles. He holds the Canada Research Chair of Energy Optimization of Intelligent Transport Systems and the Noovelia Research Chair of Intelligent Navigation of Autonomous Industrial Vehicles. He developed expertise in the optimization and the intelligent control of vehicular applications. His research interests include optimizing energy systems for vehicle applications, advanced driver assistance techniques, and intelligent vehicle navigation taking into account Canadian climatic conditions. He has a member of the Hydrogen Research Institute. He is a member of the Order of Engineers of Quebec. In 2019, his team received the First Innovation Prize in partnership with DIVEL, awarded by the Association des Manufacturiers de la Mauricie et Center-du-Québec for the development of an autonomous and natural navigation system. In 2017, he received the Environment Prize at the Gala des Grands Prix d'excellence en transport from the Association québécoise du Transport (AQTr) for the development of hydrogen range extenders for electric vehicles. He is the Winner of the Canada General Governor Gold Medal, in 2003. He was the Co-President and the President of the technical committee of the IEEE International Conferences on Vehicular Power and Propulsion, in Chicago, USA, in 2018, and in Hanoi, Vietnam, in 2019.

ALI AMAMOU (Member, IEEE) received the B.S. degree in industrial computing and automatic science from the National Institute of Applied Sciences and Technology, Tunis, Tunisia, in 2013, the M.S. degree in embedded systems science from Arts et Métiers ParisTech University, Aix-en-Provence, France, in 2014, and the Ph.D. degree in electrical engineering from Université du Québec à Trois-Rivières (UQTR), QC, Canada, in 2018. In May 2018, he started as a Postdoctoral Fellow with the Hydrogen Research Institute. His research interests include the optimization of energy systems for stationary and mobile applications, hybridization of energy sources for vehicular applications, and eco-energy navigation of the low-speed autonomous electric vehicle.

KODJO AGBOSSOU (Senior Member, IEEE) received the B.S., M.S., and Ph.D. degrees in electronic measurements from Université de Nancy I, France, in 1987, 1989, and 1992, respectively. He was a Postdoctoral Researcher and a Lecturer with the Electrical Engineering Department, Université du Québec à Trois-Rivières (UQTR), from 1993 to 1994 and from 1997 to 1998, respectively. He was the Director of the Graduate Studies in Electrical Engineering, UQTR, from 2002 to 2004. He was the Head of the Department of Electrical and Computer Engineering Department, UQTR, from 2007 to 2011. He was the Head of the Engineering School, UQTR, from 2011 to 2017, where he is currently the Hydro-Québec Research Chair of Transactive Management of Power and Energy in the Residential Sector, and the Chair of the Smart Energy Research and Innovation Laboratory. He is a member of the Hydrogen Research Institute and Research Group "GREI," UQTR. He is the author of more than 325 publications and has four patents and two patent pending. His research interests include renewable energy, the use of hydrogen, home demand side management (HDSM), integration of energy production, storage and electrical energy generation systems, connection of electrical vehicle to the grids, and control and measurements. Since 2015, he has been the Sub-Commitee Chair of the Home and Building Energy Management of Smart Grid Technical Committee and IEEE Industrial Electronics Society (IES).